HHS Public Access

Author manuscript

Cancer Immunol Immunother. Author manuscript; available in PMC 2021 May 01.

Published in final edited form as:

Cancer Immunol Immunother. 2020 May ; 69(5): 731–744. doi:10.1007/s00262-020-02504-z.

Nonlinear response to cancer nanotherapy due to macrophage interactions revealed by mathematical modeling and evaluated in a murine model via CRISPR-modulated macrophage polarization

Fransisca Leonard[a,+], **Louis T. Curtis**[b,+], **Ahmed R. Hamed**[a,c], **Carolyn Zhang**[a], **Eric Chau**[a], **Devon Sieving**[a], **Biana Godin**[a,d,*], **Hermann B. Frieboes**[e,f,g,h,*]

[a]Department of Nanomedicine, Houston Methodist Research Institute, Houston, TX USA

[b]Department of Bioengineering, University of Louisville, Louisville, Louisville, KY, USA

[c]Pharmaceutical and Drug Industries Research Division, National Research Centre, Giza, Egypt

[d]Department of Obstetrics and Gynecology, Houston Methodist Hospital, Houston, TX, USA

[e]Department of Bioengineering, University of Louisville, Louisville, KY, USA

[f]James Graham Brown Cancer Center, University of Louisville, Louisville, KY, USA

[g]Department of Pharmacology & Toxicology, University of Louisville, Louisville, KY, USA

[h]Center for Predictive Medicine, University of Louisville, Louisville, KY, USA

Abstract

Tumor associated macrophages (TAMs) have been shown to both aid and hinder tumor growth, with patient outcomes potentially hinging on the proportion of *M*1, pro-inflammatory/growth-inhibiting, to *M*2, growth-supporting, phenotypes. Strategies to stimulate tumor regression by promoting polarization to *M*1 are a novel approach that harnesses the immune system to enhance therapeutic outcomes, including chemotherapy. We recently found that nanotherapy with mesoporous particles loaded with albumin-bound paclitaxel (MSV-nab-PTX) promotes macrophage polarization towards *M*1 in breast cancer liver metastases (BCLM). However, it remains unclear to what extent tumor regression can be maximized based on modulation of the

[*]**Co-Corresponding authors:**Biana Godin: Dept. of Nanomedicine, Houston Methodist Research Institute, R8-213, 6670 Bertner St., Houston, TX, 77030, USA. Phone: 713-441-7329. bgodin@houstonmethodist.org; Hermann Frieboes: Dept. of Bioengineering, University of Louisville, Lutz Hall 419, Louisville, KY 40292, USA. Phone: 502-852-3302. hbfrie01@louisville.edu.
[+]Equal contribution

Author Contributions: Study conception and design: FL, LC, BG, HF; Experiments: FL, AH, BG, DS, EC, CZ; CRISPR liposome system development: FL; Mathematical model implementation and testing: LC, HF; Data collection and analysis: FL, LC, AH, BG, HF, DS, EC, CZ; Manuscript preparation and revision: FL, LC, BG, HF.

Conflicts of Interest: The authors have no conflicts to disclose.

Ethical Approval and Ethical Standards: *In vivo* mouse studies were performed in accordance with the Houston Methodist Research Institute Institutional Animal Care and Use Committee (IACUC - approval number: AUP-0617-0020). The animal research was conducted in full compliance with federal, state and local regulations and institutional policies.

Animal Source: Balb/c mice (6–8 weeks, females) were purchased from Jackson laboratory for all of the animal experiments in this study.

Cell Line Authentication: 4T1 mouse breast cancer cells were purchased from the American Type Culture Collection (ATCC) (Manassas, VA, USA), which tests and authenticates the cells in its collection.

macrophage phenotype, especially for poorly perfused tumors such as BCLM. Here, for the first time a CRISPR system is employed to permanently modulate macrophage polarization in a controlled *in vitro* setting. This enables the design of 3D co-culture experiments mimicking the BCLM hypovascularized environment with various ratios of polarized macrophages. We implement a mathematical framework to evaluate nanoparticle-mediated chemotherapy in conjunction with TAM polarization. The response is predicted to be not linearly dependent on the *M*1:*M*2 ratio. To investigate this phenomenon, the response is simulated via the model for a variety of *M*1:*M*2 ratios. The modeling indicates that polarization to an all-*M*1 population may be less effective than a combination of both *M*1 and *M*2. Experimental results with the CRISPR system confirm this model-driven hypothesis. Altogether, this study indicates that response to nanoparticle-mediated chemotherapy targeting poorly perfused tumors may benefit from a fine-tuned *M*1:*M*2 ratio that maintains both phenotypes in the tumor microenvironment during treatment.

Précis

Experiments are combined with mathematical modeling to evaluate cancer nanotherapy response as a function of macrophage polarization in the tumor microenvironment. Results indicate that presence of both *M*1 and *M*2 phenotypes may benefit nanotherapy.

Keywords

Cancer immunotherapy; macrophage polarization; nanotherapy; breast cancer liver metastases; mathematical modeling; computational simulation

Introduction

Breast cancer disseminates to the liver in approximately 30–50% of patients suffering from metastatic disease [1]. Unfortunately, breast cancer liver metastasis (BCLM) median survival is 4.23 months, which compares unfavorably with metastases at other sites (e.g. lung 6–15 months, bone 33–48 months, and isolated soft tissue metastases median survival > 50 months) [1]. Despite recent developments in radiation, surgical techniques, and chemo- and target-specific immune/hormone therapies, BCLM remains a leading cause of mortality. In particular, the complexity of the BCLM microenvironment has hindered the development of efficacious chemotherapeutic strategies [2]. As the liver has a dense network of capillaries reaching inner cells and efficiently providing oxygen and soluble nutrients, BCLM do not initially rely on angiogenesis for survival but rather on the existing vasculature in the surrounding parenchyma [3]. At later stages, these metastases can also change the surrounding microenvironment via angiogenesis [4], as has been observed clinically [5]. Hypo-perfusion limits diffusive transport into BCLM, as is clinically observed via MRI (magnetic resonance imaging) by the lack of contrast agent permeation yielding hypo-attenuating lesions [6]. Experimental evidence supports the notion that hypovascularization makes BCLM less susceptible to chemotherapeutic agents [7]. We have previously observed that impaired vascularity in BCLM prevents macromolecules from fully penetrating these lesions [8]. Inadequate transport is especially acute with high molecular weight (HMW) molecules and particles, as has been shown for ^{m99}Tc microaggregated albumin [9].

The complexity of BCLM further leads to dynamic changes in the cells of the tumor microenvironment (TME), especially in tumor associated macrophages (TAM) [10, 11]. TAM can be locally polarized to pro- or anti-inflammatory phenotypes, based on stimuli in the TME [12, 13]. The *M*1 phenotype favors an anti-tumor immune response [14], characterized by release of pro-inflammatory cytokines, such as IL-1, −6 and −12, TNFα, and reactive oxygen species (ROS), and expression of inducible nitric oxide synthase [15]. The *M*2 phenotype suppresses inflammation, favoring the formation of tumor stroma and neovasculature in a wound healing-type of response [16, 17], and thus promotes tumor development [18, 19]. Therapeutically-induced macrophage polarization to *M*1 has been shown to inhibit cancer progression and metastasis [20], and has become a goal for immunotherapeutic strategies targeting macrophage populations. Recent examples include carboxyl- and amino-functionalized polystyrene nanoparticles [21] and immunostimulatory agents such as RRx-001 (ABDNAZ) [22]. For breast cancer, immunotherapy involving checkpoint inhibitors or cancer vaccines in combination with established treatment strategies is undergoing promising evaluation [23].

As TAM tend to accumulate near hypoxic tissue, which is difficult to reach via vascular-borne molecules [24], we have recently evaluated taking advantage of their presence in the TME to overcome the limitations of therapeutics targeting hypo-perfused lesions. We have shown that shifting the transport of a chemotherapeutic drug from circulation towards TAM in BCLM can significantly improve outcomes and survival benefits [8, 25]. As professional phagocytes, macrophages recognize circulating solid particles, and have been shown to be a suitable target for intravenously administered nanotherapeutics. As terminally differentiated cells, macrophages are unaffected by most anti-cancer therapeutics, and, thus, can act as sources of drug in the vicinity of hypo-perfused tumor tissue, especially for HMW therapeutics.

In this study, we develop an interdisciplinary framework to facilitate effective analysis of immunotherapy aiming to affect macrophage polarization in BCLM in order to maximize the cytotoxic effect of HMW-based therapeutics. As a purely empirical approach would be insurmountable due to the complex interaction between nanotherapies, drugs, cells, and the TME, we employ both experimental and computational approaches to evaluate therapeutic response by shifting the transport of therapeutics towards macrophages in the TME while inducing polarization towards the *M*1 phenotype. In particular, we employ for the first time a CRISPR (clustered regularly interspaced short palindromic repeats) system to permanently modulate macrophage polarization. This modification allows study with varying ratio of *M*1 and *M*2 macrophages in a controlled *in vitro* environment. The experimental component is performed in a 3D co-culture that mimics the hypovascularized TME of BCLM, as previously reported [8, 25]. To enable enrichment of the *M*1 phenotype, we use liposomes loaded with CRISPR complex targeting RICTOR, rapamycin-insensitive companion of mTOR (mammalian target of rapamycin). Although several factors and pathways are involved in macrophage polarization, in our studies we have discovered that CRISPR-RICTOR-Liposomes are one of the most efficient systems to prevent polarization to the *M*2 phenotype [26]. RICTOR is an adapter protein in the mTORC2 complex, and has been shown to influence differentiation of immunosuppressive *M*2 macrophages [27, 28]. We have found that knockdown of the RICTOR gene can block *M*2 differentiation and redirect

the polarization towards the *M*1 subtype, even when subjected to pro-*M*2 stimulatory influences in the TME.

Materials and Methods

Experimental System for Cancer Cell and Macrophage Co-Culture

1. Cell Culture—4T1 mouse breast cancer cells were cultured in MEM (Minimum Essential Medium) with addition of 10% FBS (fetal bovine serum), 1% antibiotic/antimycotic, 1% GlutaMAX, 1% NEAA (non-essential amino acids), 1% MEM vitamin, and 1% sodium pyruvate supplements and maintained in humidified atmosphere at 37°C and 5% CO2.

Mouse macrophages were obtained by isolation from hind leg bone marrow from Balb/c mice (6–8 weeks, females), as previously described [25]. Briefly, mouse bone marrow was extracted by flushing with syringe, washed twice with PBS (phosphate-buffered saline), and erythrocytes were lysed by red blood cell lysis buffer (Sigma, USA). Cells were filtered with a 70μm filter (BD Lifesciences, USA). To initiate differentiation to resting macrophages (*M*0), cells were incubated with macrophage medium, containing 10% FBS and 1% penicillin/streptomycin in RPMI 1640 medium. Further differentiation of macrophages was initiated by incubation in relevant media with following addition of factors: 50ng/mL IFN-γ and 20 ng/mL LPS for *M*1 macrophage differentiation, and 50 ng/mL IL-4 and 50 ng/mL M-CSF for *M*2 macrophage differentiation.

2. crRNA production by *in vitro* transcription—CRISPR crRNA sequences targeting RICTOR were designed for the use with Cas12a using benchling tool (benchling.com/crispr). Template oligonucleotides in reverse complement sequence which included T7 promoter were ordered from Eurofins Genomics (Louisville, KY). gRNA (guide RNA) were obtained by transcribing template oligonucleotides using MEGAscript™ T7 Transcription Kit (Invitrogen, Carlsbad, CA) according to manufacturer's protocol. Produced crRNA was purified using Oligo Clean & Concentrator™ (Zymo Research, Irvine, CA). crRNA concentration was measured by assessing the absorption at 260nm using Take3 plates and Synergy H4 Hybrid Reader (Biotek, Winooski, VT).

3. CRISPR liposome design and characterization—CRISPR liposomes were designed to enrich the population of *M*1 macrophages through RICTOR molecular pathway targeting (CRISPR-RICTOR-Liposomes), which prevents macrophage differentiation into *M*2 phenotype. Liposomes were prepared using lipid hydration-extrusion method as previously described [29]. Briefly, 3.62 mg soybean phosphatidylcholine (Lipoid S100, Lipoid, Germany), and 0.88 mg 1,2-dioleoyl-3-trimethylammonium-propane (chloride salt) (DOTAP) (Avanti Polar Lipids, Alabama, USA) were dissolved in 5 mL ethanol. Solvent was evaporated for 30 minutes at 41°C and 150 rpm using rotary evaporator (Rotavapor, Buchi, Switzerland). Resulting thin film was rehydrated with 0.5 mL PBS pH 7.2, and further sonicated intermittently for 15 min using Branson 1510 bath sonicator (Branson, Danbury, CT) to create a homogeneous dispersion. CRISPR systems were prepared by mixing 1μg Cas12a nuclease (Integrated DNA Technologies, Coralville, IA) to 400 ng sgRNA (single-guide RNA) in 50μL serum free MEM medium for 5 minutes and adding this

mixture to 2μL of liposome dispersion. CRISPR-RICTOR-liposome size and zeta potential were assessed by dynamic light scattering using Zetasizer instrument (Malvern, Worcestershire, UK). Analysis was conducted in triplicates.

4. Characterization of CRISPR effect on macrophages—Undifferentiated primary macrophages were seeded on 16-well chamber slides (Nunc™ Lab-Tek™) with 30,000 cells/cm^2. CRISPR-RICTOR-liposomes were added to each well at 5μL liposome/mL, and cells were kept overnight in incubation. After 24h, the medium was changed and samples were stimulated with IL-4 and M-CSF to induce *M2* differentiation. After 48h of incubation, cells were fixed with 4% paraformaldehyde for 30 mins at 4°C. Macrophages were stained with 2.5 μg/mL rat anti-mouse CD80 primary antibody (Thermo Fisher Scientific, Waltham, MA), Alexa Fluor 568-goat anti-rat IgG secondary antibody, and FITC-rat anti-mouse CD204 antibody (Abcam, Cambridge, UK) for macrophage phenotype analysis, and counterstained with DAPI (4',6-diamidino-2-phenylindole) for nucleus stain. Cells were analyzed using Nikon A1 confocal microscope (Nikon Inc., Melville, NY, USA) and macrophage phenotypes were assessed with NIS-Elements software (Nikon Inc.).

5. Western blot analysis—Protein expression of CRISPR target RICTOR was analyzed in bone marrow-derived macrophages via Western blot. Isolated mouse macrophage cells were seeded onto 6-well plates and incubated with CRISPR-Liposome targeting RICTOR for 48 hours. At the end of incubation, semi-adherent and adherent cells were collected, centrifuged (200×g for 5 min), and the resulting cell pellet was washed with ice-cold PBS before lysing with radioimmunoprecipitation assay buffer with Halt™ protease and phosphatase cocktail (Thermo Scientific, USA) and left on ice for 20 min. Combined cell lysates were briefly sonicated at 20% amplitude for 10 sec using a probe sonicator (QSonica, LLC, Newton, CT, USA). Sonicated lysates were centrifuged (15,000 ×g for 20 min). Supernatants (cell lysates) were collected and used for protein determination using a Pierce™ BCA (bicinchoninic acid) kit (Thermo Scientific, USA), following the manufacturer instructions. Aliquots of cell lysates were denatured at 95°C for 5 min after the addition of 6× Laemmli sample buffer (Alfa Aesar, MA, USA). Proteins in cell lysates were resolved by electrophoresis on a 3–8% Tris-Acetate gels (NuPage™, Invitrogen, USA) using a constant voltage of 150 V for 1 h. Resolved proteins were blotted onto PVDF (polyvinylidene fluoride) membrane using iBlot™ stacks at 20V for 10 min using a semi-dry iBlot™ system (Invitrogen, USA). Blots were then blocked with 5% bovine serum albumin (BSA) in Tris buffered saline solution containing 0.1% Tween 20 (TBST) for 1 h at room temperature. Probing with primary antibodies were then started under gentle shaking overnight at 4°C (RICTOR rabbit monoclonal antibody, Cell Signaling Technology, 1:1000 dilution in 5% BSA in TBST and mouse monoclonal β-actin antibody (Invitrogen), 1:10000 in 5% BSA). Blots were then washed using TBST (3 × 5 min, room temp) and probed with appropriate HRP- (horseradish peroxidase) conjugated anti rabbit secondary antibodies for RICTOR (Cell Signaling Technology) and HRP conjugated antimouse β-actin antibody (Invitrogen). Membranes were then washed as above in TBST. Protein bands were visualized using Forte™ ECL (enhanced chemiluminescence) kit (EMD Millipore, MA, USA) using manufacturer instructions. Blots were imaged using a ChemiDoc XRS+ CCD (charge-coupled device) Imager (BioRad, USA). Densitometric analysis of images were

performed using VisionWorks LS™ analysis software V8.20 (UVP, LLC) for RICTOR bands and normalized to corresponding β-actin intensity. Data were analyzed for significance ($P<0.05$) using student t-test on GraphPad Prism software V8.0 (San Diego, USA).

6. RNA isolation and qPCR analysis—Macrophages were stimulated to differentiate into *M*2 phenotype with IL-4 and M-CSF for 5 days before the experiment. Macrophages were then treated with CRISPR-RICTOR-liposomes and cultured in *M*2 medium to maintain an environment favorable for differentiation to *M*2. After 4 hours of treatment, the total RNA was isolated from macrophages using RNeasy Mini Kit (Qiagen, Hilden, Germany), followed by reverse transcription using QuantiTect® Reverse Transcription Kit (Qiagen). Resulting cDNA (complementary DNA) was diluted in nuclease-free water before real-time PCR (polymerase chain reaction) step. mRNA (messenger RNA) levels were measured using QuantiTect® SYBR® Green PCR Kit (Qiagen) and StepOnePlus™ Real-Time PCR System (Applied Biosystems™). Gene expressions were normalized to the expression of corresponding β-actin housekeeping gene.

7. Efficacy studies in 3D TME co-culture model of breast cancer spheres and macrophages—4T1 mouse breast cancer cell tumor spheres were generated using Bio-Assembler™ system based on protocols we reported previously [8, 25]. For cytotoxicity studies, spheroids were grown to ~450–500 μm diameters in 96-well plate. Macrophages were treated with CRISPR-RICTOR-liposomes one day before co-culture for blocking differentiation to *M*2. Another batch of macrophages was differentiated to *M*2 according to the above protocol. On the day of co-culture, both macrophages were tested for their phenotype with rat anti-mouse CD80 antibody (Thermo Fisher Scientific, Waltham, MA) confirming *M*1 phenotype and rabbit anti-mouse CD204 antibody (Abcam, Cambridge, UK) confirming *M*2 phenotype. After phenotype confirmation, macrophages were harvested and co-cultured with 4T1 spheroids with different ratio of CRISPR-RICTOR- liposome-treated macrophages (*M*1) and *M*2 macrophages, with 2×10^3 macrophages in total.

In the efficacy study with mesoporous particles loaded with albumin-bound paclitaxel (MSV-nab-PTX), *M*1 and *M*2 macrophages were seeded in co-culture with 4T1 spheroids at different ratios of *M*1 and *M*2, similar to the previous setup. Further, MSV-nab-PTX was added to the co-culture at a dose equivalent to ~30 ng of PTX (paclitaxel). After 48 or 72 h, the 4T1 spheres were harvested and analyzed for viability using CellTiter-Glo 3D Cell Viability Assay (Promega, Madison, Wisconsin) according to manufacturer's protocol.

8. Evaluation of CRISPR-RICTOR-Liposomes effect *in* vivo in breast cancer model—Breast cancer model was generated by orthotopic injection of 10^5 4T1 cells/100 μL PBS in Balb/c mice (6–8 weeks, females). Tumors were grown for 10 d prior to injection of CRISPR-RICTOR Liposome systems. Animals were randomized into treatment and control groups (n=6), and 100μL of CRISPR-RICTOR-Liposomes or 100μL PBS (control) were injected intratumorally to the lesion. Mice were sacrificed after 24 h. Tumors were harvested and frozen in OCT (optimal cutting temperature) compound followed by cryo-sectioning and staining for CD80 (*M*1) and CD206 (*M*2) macrophage markers. Slides were stained with Alexa Fluor647-anti mouse CD80 and Alexa Fluor488-anti mouse CD206

antibodies (Abcam, Cambridge, UK), and counterstained with DAPI (Thermo Fisher, Waltham, MA). Colocalizations of CD80 in macrophages were confirmed by co-staining of CD80 and Alexa Fluor488-anti mouse CD11b antibodies (Abcam, Cambridge, UK).

9. Mathematical model of BCLM response to therapy as a function of macrophage polarization—The model presented in [8, 25] simulated the tumor response to MSV-nab-PTX nanoparticles uptaken by macrophages. This model was extended here to simulate the effect of a hypothetical agent affecting macrophage polarization (AAMP) towards *M*1 or *M*2 subtypes. The main model parameters are summarized in Supplementary Table 1, with values previously calibrated in [8, 25, 30, 31] to achieve biologically meaningful results. The model includes the vasculature in the extratumoral space because it represents the *in vivo* condition of the metastatic lesions in the liver, for which the extratumoral space is vascularized. The angiogenesis model component simulates the model by [32] and is based on [30, 31]. Oxygen and vasculature-related parameters are as in [2,3]. A simplified liver vascular organization composed of square elements is simulated, acknowledging that in biological reality these elements are heterogeneously delineated by the sinusoids between the portal tracts and central veins at high density.

The model was calibrated following [8]. Details of the numerical implementation are in [30] and references therein, including [31].

Simulation of Macrophages: As in [33], undifferentiated macrophages extravasate from the vasculature in proportion to local concentration of macrophage chemoattractants (e.g., pro-angiogenic factors released by tumor cells). They migrate through the interstitium following gradients of oxygen, chemoattractants, and pressure, as described in [33]. Polarization into *M*1 or *M*2 subtypes occurs in the vicinity of the tumor microenvironment based on the ratio of pro-*M*1 and pro-*M*2 macrophage factors released by viable tumor cells [8, 25]. The number of macrophages and their localization in the simulations is stochastic, and thus variability is introduced in the *M*1:*M*2 ratios. Simulations were run n=5 in order to obtain statistically significant results.

*M*1 macrophages are simulated to penetrate deeper than *M*2 subtypes into tumor tissue, as shown in Supplementary Fig 1(a) (showing an average macrophage number), to replicate this effect observed in our recently published experiments [25]. This effect is modeled via an additional chemoattractant with increasing concentration towards the center of the lesion selectively influencing *M*1 movement [25].

Further, we have experimentally observed [25] that the presence of MSV-nab-PTX shifts the ratio of *M*1 to *M*2 macrophages to be 1.2:1.0. This effect is calibrated in the model by simulating a one-time bolus injection of MSV-nab-PTX into the system. Supplementary Fig 1(b) shows the accumulation of MSV-nab-PTX loaded *M*1 and *M*2 macrophages in the simulated tumor over time. The number of drug-loaded macrophages peaks in the tumor within 24h post MSV-nab-PTX injection, and decreases to zero by 36h. Although macrophages *in vivo* have longer and more variable lifespans in the TME, this timeframe provides a consistent period for the evaluation of macrophage polarization and its effects on the growing tumor.

Macrophages act as point sources of drug to simulate the release of paclitaxel from the MSV-nab-PTX system, as described in [8]. This drug is diffused in the TME to induce local cytotoxicity [8, 25]. For simplicity, drug uptake by tumor tissue, death effect, and washout from the interstitium are simulated to take effect immediately [34]. Additionally, *M*1 macrophages induce cytotoxicity while *M*2 promote tumor cell proliferation [25, 33].

Simulation of Agent Inducing Polarization to *M*1 Phenotype: Macrophage polarization to the *M*1 phenotype is driven by simulating a bolus infusion of a hypothetical "agent affecting macrophage polarization" (AAMP), here generically named *N*:

$$\frac{dN}{dt} = \nabla \cdot (D_N \nabla N) + \lambda^N_{release}(t, \mathbf{1}_{vessel}) - \lambda^N_{decay} N$$

AAMP with diffusivity D_N is released at rate $\lambda^N_{release}$ from vessels at location $\mathbf{1}_{\text{vessel}}$ (of value 1 if a vessel is present and 0 otherwise), and decays at rate λ^N_{decay}, acting locally on undifferentiated macrophages to promote their conversion to the *M*1 phenotype. The likelihood of conversion is proportional to the local concentration of *N* and its strength, λ^N_{effect} [35]. This strength starts with a value of 0 to attain a *M*1:*M*2 ratio of 1.2:1 (as experimentally observed when MSV-nab-PTX are present [25]), and is incremented in steps of 80 to achieve an increasing magnitude of these ratios, as depicted in Supplementary Fig 2.

10. Statistical Analysis—Data were statistically analyzed using student t test on GraphPadPrism software. P-values below 0.05 were considered significant, and $p<0.01$ as very significant.

Results

Since macrophage polarization is a dynamic process influenced by the TME, in order to achieve a stable phenotype we used here for the first time a CRISPR system targeting RICTOR that allows to block *M*2 and to induce *M*1 macrophage differentiation [27, 28, 36]. As this modulation of *M*1 to *M*2 ratio can only be achieved in a controlled *in vitro* environment, a 3D co-culture system that mimics the hypovascularized TME of BCLM was employed, as previously reported [8].

Treatment with CRISPR-RICTOR-Liposome was able to knock down RICTOR expression, as shown in western blot in Fig 1(a) and quantified in Fig 1(b). Fluorescence images in Fig 1(c) show that a stable *M*1 phenotype was achievable even when stimulated to differentiate towards *M*2. Further, the reprogramming was assessed by measurement of mRNA expression of inflammatory- related genes. Treatment of *M*2-differentiated macrophages with CRISPR-RICTOR-Liposomes caused a switch to an *M*1-like subtype, as indicated by the increase in expression of pro-inflammatory genes. As shown in Fig 1(d), expression of MCP-1, MIP-1α, MIP-1β, RANTES, KC, and IL-1β were significantly elevated (up to 100-fold induction). On the other hand, expression of anti-inflammatory cytokine IL-10 was reduced, as expected when macrophage polarization shifts to a more pro-inflammatory *M*1 subtype. Differentiation of CRISPR-treated macrophages was evaluated following cell

stimulation with IL-4 and M-CSF, which normally induces *M*2 differentiation. Cells not treated with IL-4 and M-CSF showed preferential differentiation towards the *M*1 macrophage phenotype, with ~75% *M*1 macrophages in both CRISPR treated and untreated control. CRISPR treatment was very effective in blocking *M*2 differentiation upon stimulation with IL-4 and M-CSF, with the cells retaining ~85% of the *M*1 phenotype, while all cells that did not undergo genetic editing differentiated towards the *M*2 phenotype (Fig 1(e)).

The ability of the CRISPR-RICTOR-Liposome treatment to shift the macrophage phenotype was evaluated in an *in vivo* model of breast cancer. The treatment caused a more than 12-fold increase in fluorescence intensity of the *M*1 macrophage marker CD80 in the tumor tissue as compared to the tumor injected with PBS (Supplementary Fig 3). CD80 has been reported as a robust phenotypic marker for human $M\Phi_{IFN\text{-}\gamma}$ (*M*1 phenotype) macrophages [37]; however, as it can also be expressed by other immune cells (e.g., B and T cells), we confirmed that the signal originated with *M*1 macrophages by co-staining with the CD11b pan-macrophage marker (Supplementary Fig 4). The co-localization of CD80 and CD11b fluorescent signals shows that the vast majority of CD80+ cells were *M*1 macrophages in the CRISPR-Lip treated tumor. In the untreated control, while CD11b staining intensity was similar to the treated tumor, there was a very weak signal of CD80+, as expected since most of the macrophages in the tumor were *M*2-like phenotype. The figure further shows that the level of cells expressing the *M*2 marker CD206 was not significantly affected by the treatment. CD206 is a well-accepted (classical) and very specific marker for *M*2 differentiation [38, 39], which has been used as a benchmark to evaluate new *M*2 candidate markers [40].

Next, we evaluated the response to MSV-nab-PTX at different *M*1:*M*2 ratios. We confirmed that the macrophage phenotypes as well as the *M*1:*M*2 ratios in the presence of cancer spheroids remained stable for the duration of the experiments, equaling the initial ratios introduced at t=0 (Supplementary Fig 5). The ratios in the figure refer to macrophages differentiated towards the *M*2 phenotype vs. macrophages arrested in the *M*1 phenotype using CRISPR. In Fig 2, varying strengths of a hypothetical “agent affecting macrophage polarization” (AAMP) that shifts macrophage polarization towards the *M*1 subtype were mimicked by varying the ratio of *M*1:*M*2 subtypes in the spheroid co-cultures. When the cells were not treated with MSV-nab-PTX, cancer cell viability increased as this ratio decreased, plateauing for values lower than 1:1 for both 48 and 72h treatment durations. In contrast, the MSV-nab-PTX case was non-uniform with respect to this ratio. The lowest cell viability for 48h exposure was for the *M*1-only case and increased with higher numbers of *M*2, with *M*1:*M*2 ratios of 1500:500 and 1000:1000 showing statistically similar results. For 72h, an *M*1:*M*2 ratio of 1500:500 achieved lower viability than 2000:0 (all *M*1), indicating that the presence of the *M*2 subtype augments the therapeutic efficacy. Likewise, the ratio of 0:2000 (all *M*2) yields=ed lower viability than the 500:1500 ratio.

To more systematically explore the effect of macrophage polarization on the response of hypovascularized cancer lesions to MSV-nab-PTX, we applied mathematical modeling to simulate BCLM growth and treatment response. With the model parameters calibrated as described in Methods, a representative BCLM lesion was first grown by the model to a

diameter ~400 μm (Supplementary Fig 6). As the lesion grows, tissue regions with adequate access to oxygen and nutrients are able to proliferate while regions with inadequate access become hypoxic. The dense liver capillary network is modeled by the rectangular grid, with irregular sprouts generated through angiogenesis during the lesion progression.

During the tumor growth process, individual macrophages are recruited to the vicinity of the lesion based on attraction to chemoattractants released by the hypoxic tumor cells. Based on the local TME conditions, these macrophages differentiate into *M*1 or *M*2 subtypes, which respectively either hinder or aid the tumor progression. The *M*1 macrophages release cytotoxins, e.g., nitric oxide, which affect the viability of tumor cells in their immediate vicinity. This is simulated to alter the tumor tissue proportionally to the concentration of the toxins released. Fig 3(a) shows the anti-proliferative effect of *M*1 macrophages. As the released nitric oxide from *M*1 macrophages is quickly degraded, the model simulates a cytotoxic effect in the locations of *M*1 macrophages to achieve a local effect. The effect of the nitric oxide is reflected by the tumor shrinkage compared to the initial condition (Supplementary Fig 6). Fig 3(b) shows the same situation but including MSV-nab-PTX uptake by the *M*1 macrophages 24h after therapy initiation, which accentuates the tumor shrinkage. The *M*2 macrophages release growth factors (e.g. TGF-β) that stimulate the survival and proliferation of tumor cells. This effect was simulated in the model by having the *M*2 subtypes release a generic growth factor that adds to the overall proliferation term. In the model these growth factors up-regulate the proliferation of both proliferating and hypoxic tumor tissue, which increases the overall tumor growth rate. Fig 3(c) shows the *M*2 macrophage influence on the tumor growth. In this snapshot, the macrophages are in peak concentration and predominantly distributed within the tumor or at the boundary. Fig 3(d) shows the same situation but includes MSV-nab-PTX uptake by the *M*2 macrophages 24h after therapy initiation, which now leads to substantial tumor shrinkage.

Next, we evaluated the delivery of a hypothetical AAMP to the tumor microenvironment to dynamically affect the *M*1:*M*2 polarization, which in turn alters the tumor growth characteristics. An increasing strength of AAMP was simulated to have a corresponding steady increase in the ratio of *M*1 to *M*2 macrophages. Supplementary Fig 2 summarizes the average *M*1:*M*2 ratio for different cases of λ_{effect}^{N}, the AAMP strength. As λ_{effect}^{N} is increased, the probability of AAMP causing conversion to an *M*2 macrophage is increased. With five simulation samples for each AAMP strength (n=5), there is variability in the *M*1:*M*2 ratio. This is due to the stochastic nature of macrophage production and movement through the simulated TME. Macrophages near the vasculature may have more exposure to AAMP and, thus, locally higher *M*1:*M*2 ratios. Despite this variability, an overall trend of increasing *M*1:*M*2 ratios with increasing AAMP strength is attained (Supplementary Fig 2).

The strength of AAMP increases the overall *M*1 macrophage population and decreases the *M*2 population, while both of these subtypes are also releasing albumin-bound paclitaxel (nab-PTX) in the tumor vicinity from the MSV-nab-PTX that they have taken up in the circulation. Fig 4 qualitatively displays the tumor course over 36h under exposure to AAMP therapy of medium strength (λ_{effect}^{N} = 280, for which *M*1:*M*2 is 3.0:1), while simultaneously simulating a bolus injection of MSV-nab-PTX drug-loaded nanotherapy at 0h. The MSV-

nab-PTX uptaken by the macrophages are retained near and within the lesion by the macrophage infiltration, while the nab-PTX is released from them in the tumor proximity. The hypothetical AAMP administered intravenously as a bolus injection to polarize the macrophages has its maximum concentration at t=0 hours, and is progressively washed out from the tissue. Both PTX and the macrophages reach maximal numbers later in the simulation, as shown at 12h. By 36h, the immunotherapy and PTX effects have waned, and the tumor begins to regrow.

The tumor response over time when treated with MSV-nab-PTX loaded macrophages is shown in Fig 5. A general trend of increased $M1$:$M2$ ratio leading to decreased tumor size can be seen (Fig 5(a)). When simulating the effect of $M1$ only (i.e., inactivated $M2$, Fig 5(b)) while maintaining the same proportion of macrophages, i.e., the same number of activated $M1$, the tumor response is significantly less than when the $M2$ are active (Fig 5(a)), even in the case of a high ratio of $M1$:$M2$ of 3.8:1. Thus, a dual effect of the $M2$ macrophages is predicted by the model. Since PTX is a cell-cycle inhibitor, $M2$ macrophages potentiate the effect of AAMP during treatment while also accelerating tumor recovery post treatment (Fig 5(a)). To evaluate this effect further, we simulated repeated treatment cycles with MSV-nab-PTX. For treatments every 2d (Fig 5(c) or every 3d (Fig 5(d)), the presence of both $M1$ and $M2$ subtypes yielded significantly higher tumor regression than when $M2$ macrophages were inactive.

Fig 6 summarizes the minimum tumor radius achieved by the MSV-nab-PTX bolus injection for the three treatment protocols in Fig 5 in the case of an $M1$:$M2$ ratio of 3.0:1, comparing the case when both $M1$ and $M2$ are active vs. when $M2$ is inactive. The model results indicate that the presence of the $M2$ can provide a significantly higher tumor regression, whether the MSV-nab-PTX is administered as a single dose or in multiple doses over a number of days.

Altogether, these results indicate that there may exist tumor-specific conditions for which a certain number of MSV-nab-PTX-loaded $M2$ may help to amplify the tumor response due to the $M2$ phenotype promoting tumor proliferation in the presence of cell-cycling drugs, whereas a predominantly $M1$ population would be less effective.

Discussion

Targeting macrophages in the TME is gaining recognition as a promising strategy for tumor therapy [41], with the critical role of macrophages in cancer growth, progression and immunotherapy recently reviewed in [42], highlighting the potential of innate immunity/ macrophage modulation to restrain tumor growth. Macrophages are a key cell population of the innate immune system, with the $M1$ type triggering naïve T cells to have a Th1/cytotoxic response and the $M2$ type triggering T cells to have a Th2-type response associated with antibody production [43]. Both types serve multi-faceted purposes to maintain tissue homeostasis, with the $M1$ upholding immunity against foreign threats and the $M2$ modulating tissue repair and healing. Consequently, an imbalance in either one can potentially lead to severe illness; strong $M1$ activity has been associated with auto-immune

diseases and organ rejection, while predominance of *M2* activity has been linked to tumor progression.

Multiple studies focusing on finding agents that can shift macrophage polarization from an anti-inflammatory and tumorigenic *M2* phenotype to a pro-inflammatory and anti-cancerous *M1* phenotype are underway [25, 44–46]. While modulating macrophage polarization as *a solo* therapy has shown some promise [44], pronounced clinical benefits are expected mainly in combination with standard therapy. Recently, we reported that MSV-nab-PTX nanotherapy shifts the transport of therapeutics in BCLM from circulating in the bloodstream and, thus, unable to penetrate hypo-pefused metastatic lesions, to therapeutics specifically taken up and retained/transported by macrophages into the BCLM TME to be released there [8]. Integrating both experiments and mathematical modeling, we demonstrated that the proposed nanotherapy targeting cancer cells can additionally influence macrophage polarization from *M2* to *M1* [25].

In the current study, we evaluated the response of breast cancer cells to MSV-nab-PTX in 3D co-culture mimicking the TME of hypovascularized lesions in the liver with various ratios of polarized macrophages. To enable a stable polarization of macrophages and avoid their repolarization under the dynamic biochemical stresses in the TME, CRISPR technology was utilized. Consistent with the computational simulation predictions from our previous work [25], our experimental results here confirmed that the response to the cytotoxic agent MSV-nab-PTX depends non-linearly on the *M1*:*M2* ratio. To explore this phenomenon further, we employed the mathematical modeling to analyze the effects of therapy while simulating manipulation of the macrophage phenotype via a hypothetical “agent affecting macrophage polarization” (AAMP). Although the role of macrophages in cancer therapy has been previously investigated via mathematical modeling, as recently reviewed in [47], the influence of varying macrophage phenotypes on the response to nanotherapy has had limited evaluation. The model-based finding that the *M2*-tumor interaction may have a dual role in the response to MSV-nab-PTX, initially promoting tumor death and subsequently aiding tumor recovery, highlights the nonlinear effect of the macrophage polarization in the TME during treatment. This interaction is expected to depend on nanotherapy and tumor tissue-specific conditions, including vascularization, hypoxia, and other microenvironment characteristics affecting macrophage behavior, which require further elucidation. Further, the model results suggest that immunotherapy strategies solely based on maximizing the *M1*:*M2* ratio may be less effective than protocols which establish an *M1*:*M2* proportion that first maximizes tumor regression during chemotherapeutic exposure, and then maximizes this ratio in favor of the *M1* phenotype during the tumor recovery phase.

It is to be noted that there are multiple factors in the liver metastatic TME affecting tumor growth and therapy response. These factors include, among others, liver fibrosis and activation of stellate cells, T-cell exhaustion, and enrichment of myeloid-derived suppressor cells (MDSCs). Here, we focused on the polarization of tumor-associated macrophages, which in itself may be insufficient to restrain metastatic growth. However, it is considered valuable to study each of these factors in order to understand the associated mechanisms and to explore therapeutic combinations. The results here show that the polarization of macrophages may play an important role in the planning of combinatorial therapeutic

regimens. We further note that PTX is a chemotherapeutic that targets proliferating cells; thus, differentiated cells such as macrophages are typically unaffected by PTX. We have previously shown that macrophage viability was not impacted by PTX up to 50μg/mL *in vitro*, and that macrophages in uninvolved liver were not affected by MSV-nAb-PTX treatment *in vivo* [48]. However, PTX in high concentration may induce intravellular signals that mimic lipopolysaccharides in murine macrophages [49].

The goal for effective therapy would be to deliver and maintain a therapeutic drug dose to a target site while minimizing systemic toxicity. Numerous macromolecule-based therapeutic strategies have been proposed and clinically approved in recent years to treat advanced breast cancer, including albumin-bound drug conjugates (e.g., nab-PTX or Abraxane®), various antibodies (e.g., anti-HER2 mAb (monoclonal antibody) or Trastuzumab) and genetic materials (such as siRNA (small interfering RNA), miRNA (micro RNA) and aptamers). In hypo-vascularized BCLM, these potent therapeutics are unable to be transported in cytotoxic concentrations into tumor tissue prior to their clearance from circulation. Thus, new approaches to enhance therapeutic macromolecule accumulation in hypo-perfused tumor tissue are necessary. The results in this study show that effectiveness of a cytotoxic regimen with MSV-nab-PTX, which has shown promise to overcome these transport barriers *in vitro* [8, 25] and *in vivo* [45] by leveraging phagocytic uptake by TAM in the TME, could potentially be accentuated with immunotherapy that adjusts the $M1$:$M2$ ratio to first boost tumor death during drug exposure and then to hinder tumor recovery post chemotherapy. Further work is necessary to elucidate the therapy and TME parameters that define the conditions to maximize response. The interdisciplinary framework presented here lays a first step towards the design of therapies customized to specific TME and immunological conditions.

Supplementary Material

Refer to Web version on PubMed Central for supplementary material.

Acknowledgments

Funding: Leonard acknowledges Houston Methodist Research Institute Department of Nanomedicine Innovative Grant Award and METAvivor Foundation Early Career Investigator Award. Leonard and Godin gratefully acknowledge funding from George and Angelina Kostas Research Center for Cardiovascular Nanomedicine Grant. Frieboes acknowledges partial support by the National Institutes of Health/National Cancer Institute Grant R15CA203605.

List of Abbreviations

AAMP	agent affecting macrophage polarization
BCA	bicinchoninic acid
BCLM	breast cancer liver metastasis
BSA	bovine serum albumin
CCD	charge-coupled device

cDNA	complementary DNA
CRISPR	clustered regularly interspaced short palindromic repeats
crRNA	CRISPR RNA
DAPI	4’,6-diamidino-2-phenylindole
DNA	deoxyribonucleic acid
ECL	enhanced chemiluminescence
FBS	fetal bovine serum
gRNA	guide RNA
HMW	high molecular weight
HRP	horseradish peroxidase
mAb	monoclonal antibody
MEM	minimum essential medium
miRNA	micro RNA
mRNA	messenger RNA
MRI	magnetic resonance imaging
MSV-nab-PTX	mesoporous particles loaded with nab-PTX
mTOR	mammalian target of rapamycin
nab-PTX	albumin-bound paclitaxel
NEAA	non-essential amino acids
OCT	optimal cutting temperature
PBS	phosphate-buffered saline
PCR	polymerase chain reaction
PTX	paclitaxel
PVDF	polyvinylidene fluoride
qPCR	quantitative PCR
RICTOR	rapamycin-insensitive companion of mTOR
RIPA	radioimmunoprecipitation assay
RNA	ribonucleic acid
sgRNA	single guide RNA

siRNA	small interfering RNA
TAM	tumor-associated macrophage
TME	tumor microenvironment
TBST	tris- buffered saline with Tween-20

References

1. Wyld L, et al., Prognostic factors for patients with hepatic metastases from breast cancer. British Journal of Cancer, 2003 89(2): p. 284–290. [PubMed: 12865918]
2. van den Eynden GG, et al., The multifaceted role of the microenvironment in liver metastasis: Biology and clinical implications. Cancer Research, 2013 73(7): p. 2031–2043. [PubMed: 23536564]
3. Stessels F, et al., Breast adenocarcinoma liver metastases, in contrast to colorectal cancer liver metastases, display a non-angiogenic growth pattern that preserves the stroma and lacks hypoxia. British Journal of Cancer, 2004 90(7): p. 1429–1436. [PubMed: 15054467]
4. Ma R, et al., Mechanisms involved in breast cancer liver metastasis. J Transl Med, 2015 13: p. 64. [PubMed: 25885919]
5. Braga L, et al., Does hypervascularity of liver metastases as detected on MRI predict disease progression in breast cancer patients? AJR Am J Roentgenol, 2004 182(5): p. 1207–13. [PubMed: 15100120]
6. Liu LX, Zhang WH, and Jiang HC, Current treatment for liver metastases from colorectal cancer. World J Gastroentero, 2003 9(2): p. 193–200.
7. Pezzella F and Gatter KC, Evidence Showing That Tumors Can Grow Without Angiogenesis and Can Switch Between Angiogenic and Nonangiogenic Phenotypes. J Natl Cancer Inst, 2016 108(8): djw032. [PubMed: 27059375]
8. Leonard F, et al., Enhanced performance of macrophage-encapsulated nanoparticle albumin-bound-paclitaxel in hypo-perfused cancer lesions. Nanoscale, 2016 8(25): p. 12544–52. [PubMed: 26818212]
9. Daly JM, et al., Predicting tumor response in patients with colorectal hepatic metastases. Annals of surgery, 1985 202(3): p. 384–93. [PubMed: 2931055]
10. Coussens LM and Werb Z, Inflammation and cancer. Nature, 2002 420(6917): p. 860–867. [PubMed: 12490959]
11. Balkwill F, Charles KA, and Mantovani A, Smoldering and polarized inflammation in the initiation and promotion of malignant disease. Cancer Cell, 2005 7(3): p. 211–217. [PubMed: 15766659]
12. Martinez FO, Regulators of macrophage activation. European Journal of Immunology, 2011 41(6): p. 1531–1534. [PubMed: 21607943]
13. Sica A and Mantovani A, Macrophage plasticity and polarization: in vivo veritas. The Journal of Clinical Investigation, 2012 122(3): p. 787–795. [PubMed: 22378047]
14. Jakubzick CV, Randolph GJ, and Henson PM, Monocyte differentiation and antigen-presenting functions. Nat Rev Immunol, 2017 17: p. 349–362. [PubMed: 28436425]
15. Galdiero MR, et al., Tumor associated macrophages and neutrophils in cancer. Immunobiology, 2013 218(11): p. 1402–10. [PubMed: 23891329]
16. Mills CD, Anatomy of a discovery: *m*1 and *m*2 macrophages. Front Immunol, 2015 6: p. 212. [PubMed: 25999950]
17. Sica A, et al., Tumour-associated macrophages are a distinct *M*2 polarised population promoting tumour progression: Potential targets of anti-cancer therapy. European Journal of Cancer, 2006 42(6): p. 717–727. [PubMed: 16520032]
18. Cao W, et al., Macrophage subtype predicts lymph node metastasis in oesophageal adenocarcinoma and promotes cancer cell invasion in vitro. British Journal of Cancer, 2015 113(5): p. 738–746. [PubMed: 26263481]

19. Pantano F, et al., The role of macrophages polarization in predicting prognosis of radically resected gastric cancer patients. Journal of Cellular and Molecular Medicine, 2013 17(11): p. 1415–1421. [PubMed: 24283947]
20. Georgoudaki A-M, et al., Reprogramming Tumor-Associated Macrophages by Antibody Targeting Inhibits Cancer Progression and Metastasis. Cell Reports, 2016 15(9): p. 2000–2011. [PubMed: 27210762]
21. Fuchs AK, et al., Carboxyl- and amino-functionalized polystyrene nanoparticles differentially affect the polarization profile of *M*1 and *M*2 macrophage subsets. Biomaterials, 2016 85: p. 78–87. [PubMed: 26854393]
22. Oronsky B, et al., RRx-001: a systemically non-toxic *M*2-to-*M*1 macrophage stimulating and prosensitizing agent in Phase II clinical trials. Expert Opin Investig Drugs, 2017 26(1): p. 109–119.
23. Nathan MR and Schmid P, The emerging world of breast cancer immunotherapy. Breast, 2017.
24. Lewis C and Murdoch C, Macrophage responses to hypoxia: implications for tumor progression and anti-cancer therapies. The American journal of pathology, 2005 167(3): p. 627–35. [PubMed: 16127144]
25. Leonard F, et al., Macrophage polarization contributes to the anti-tumoral efficacy of mesoporous nanovectors loaded with albumin-bound paclitaxel. Frontiers in Immunology, 2017 8: p. 693. [PubMed: 28670313]
26. Leonard F and Godin B, Agents for macrophage polarization. 2018, Houston Methodist: United States.
27. Babaev VR, et al., Loss of Rictor in Monocyte/Macrophages Suppresses Their Proliferation and Viability Reducing Atherosclerosis in LDLR Null Mice. Frontiers in Immunology, 2018 9: p. 215. [PubMed: 29487597]
28. Festuccia WT, et al., Myeloid-Specific Rictor Deletion Induces *M*1 Macrophage Polarization and Potentiates In Vivo Pro-Inflammatory Response to Lipopolysaccharide. PLOS ONE, 2014 9(4): p. e95432. [PubMed: 24740015]
29. Refuerzo JS, et al., Liposomes: a nanoscale drug carrying system to prevent indomethacin passage to the fetus in a pregnant mouse model. Am J Obstet Gynecol, 2015 212(4): p. 508 e1–7. [PubMed: 25683966]
30. Macklin P, et al., Multiscale modelling and nonlinear simulation of vascular tumour growth. Journal of Mathematical Biology, 2009 58(4–5): p. 765–798. [PubMed: 18781303]
31. Wu M, et al., The effect of interstitial pressure on tumor growth: Coupling with the blood and lymphatic vascular systems. Journal of Theoretical Biology, 2013 320: p. 131–151. [PubMed: 23220211]
32. McDougall SR, Anderson ARA, and Chaplain MAJ, Mathematical modelling of dynamic adaptive tumour-induced angiogenesis: Clinical implications and therapeutic targeting strategies. Journal of Theoretical Biology, 2006 241(3): p. 564–589. [PubMed: 16487543]
33. Mahlbacher G, et al., Mathematical modeling of tumor-associated macrophage interactions with the cancer microenvironment. J Immunother Cancer, 2018 6(1): p. 10. [PubMed: 29382395]
34. van de Ven AL, et al., Integrated intravital microscopy and mathematical modeling to optimize nanotherapeutics delivery to tumors. AIP advances, 2012 2(1): p. 11208. [PubMed: 22489278]
35. Curtis LT and Frieboes HB, Modeling of Combination Chemotherapy and Immunotherapy for Lung Cancer, in 41st Annual International Conference of the IEEE Engineering in Medicine and Biology Society (EMBC) 2019, IEEE: Berlin, Bermany p. 273–276.
36. Hallowell RW, et al., mTORC2 signalling regulates *M*2 macrophage differentiation in response to helminth infection and adaptive thermogenesis. Nature Communications, 2017 8: p. 14208.
37. Ambarus CA, et al., Systematic validation of specific phenotypic markers for in vitro polarized human macrophages. J Immunol Methods, 2012 375(1–2): p. 196–206. [PubMed: 22075274]
38. Porcheray F, et al., Macrophage activation switching: an asset for the resolution of inflammation. Clin Exp Immunol, 2005 142(3): p. 481–9. [PubMed: 16297160]
39. Maeda A, et al., Poly(I:C) stimulation is superior than Imiquimod to induce the antitumoral functional profile of tumor-conditioned macrophages. Eur J Immunol, 2019 49(5): p. 801–811. [PubMed: 30779113]

40. Jablonski KA, et al., Novel Markers to Delineate Murine *M*1 and *M*2 Macrophages. PLoS One, 2015 10(12): p. e0145342. [PubMed: 26699615]
41. Brown JM, Recht L, and Strober S, The Promise of Targeting Macrophages in Cancer Therapy. Clin Cancer Res, 2017 23(13): p. 3241–3250. [PubMed: 28341752]
42. Mills CD, Lenz LL, and Harris RA, A Breakthrough: Macrophage-Directed Cancer Immunotherapy. Cancer Res, 2016 76(3): p. 513–6. [PubMed: 26772756]
43. Mills CD, et al., M-1/M-2 macrophages and the Th1/Th2 paradigm. J Immunol, 2000 164(12): p. 6166–73. [PubMed: 10843666]
44. Pyonteck SM, et al., CSF-1R inhibition alters macrophage polarization and blocks glioma progression. Nat Med, 2013 19(10): p. 1264–72. [PubMed: 24056773]
45. Tariq M, et al., Macrophage Polarization: Anti-Cancer Strategies to Target Tumor-Associated Macrophage in Breast Cancer. J Cell Biochem, 2017 118(9): p. 2484–2501. [PubMed: 28106295]
46. Poh AR and Ernst M, Targeting Macrophages in Cancer: From Bench to Bedside. Front Oncol, 2018 8: p. 49. [PubMed: 29594035]
47. Mahlbacher GE, Reihmer KC, and Frieboes HB, Mathematical modeling of tumor-immune cell interactions. J Theor Biol, 2019 469: p. 47–60. [PubMed: 30836073]
48. Tanei T, et al., Redirecting transport of nanoparticle albumin-bound paclitaxel to macrophages enhances therapeutic efficacy against liver metastases. Cancer Research, 2016 76(2): p. 429–439. [PubMed: 26744528]
49. Vogel SN, Carboni JM, and Manthey CL, Paclitaxel, a Mimetic of Bacterial Lipopolysaccharide (LPS) in Murine Macrophages, in Taxane Anticancer Agents, Georg GI, Chen TT, and Ojima I, Editors. 1994, American Chemical Society p. 162–172.

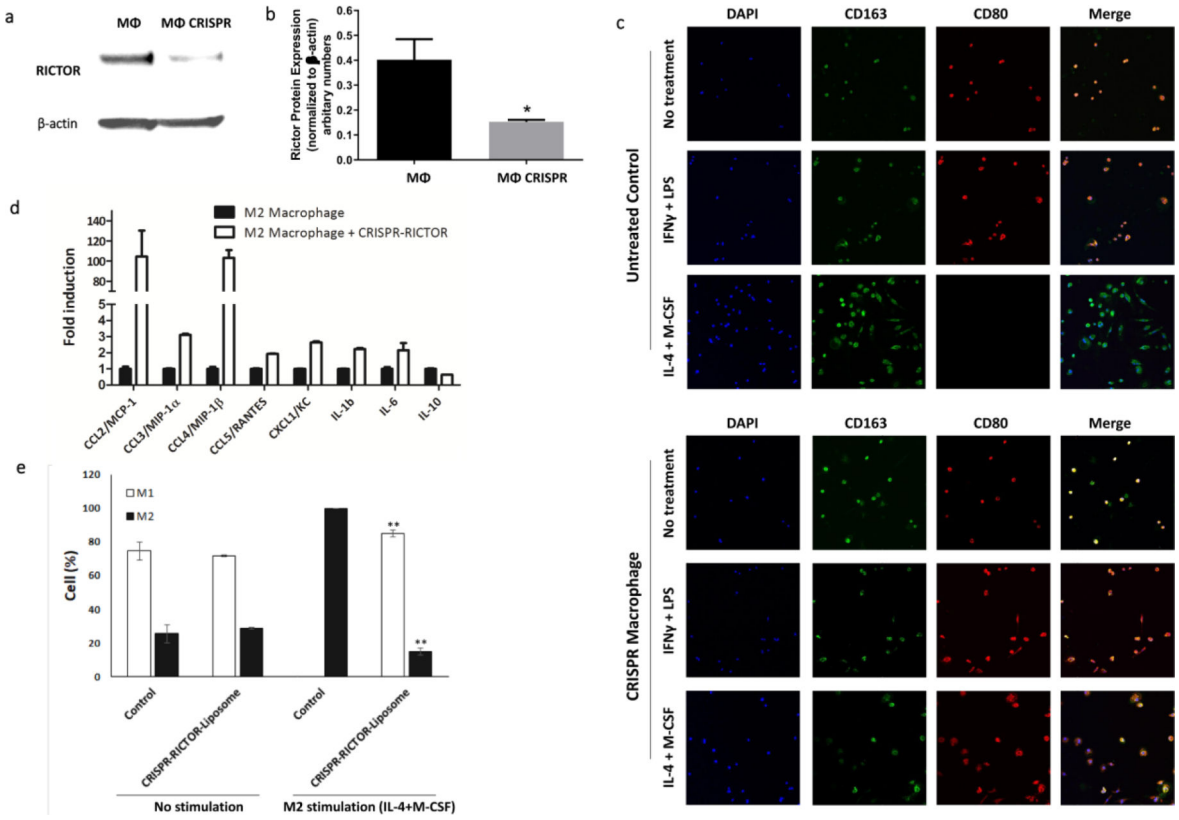

Fig 1:

Evaluation of effects of CRISPR-RICTOR-Liposome on *M2* polarized macrophages *in vitro*. (a) Immunoblotting analysis of RICTOR protein expression in untreated (*M*Φ) versus macrophages treated with CRISPR-RICTOR-Liposome (*M*Φ CRISPR). Isolated mouse macrophages were cultured, treated and analyzed by Western blot. (b) Densitometric analysis of RICTOR band intensities normalized to β-Actin. n=3, *significant to untreated macrophage control (*M*Φ) ($p<0.05$). (c) Effect on macrophage differentiation of CRISPR treatment targeting RICTOR, coupled with macrophage differentiation stimulated towards *M1* (IFNγ+LPS) or *M2* (IL-4+M-CSF). Cells were stained with CD163 (green-*M2* marker) and CD80 (red-*M1* marker). (d) mRNA expression from *M2* macrophages with and without treatment with CRISPR-RICTOR-Liposome, measured via qPCR (n=4). (e) Quantitative analysis of cell phenotype. Scale bar = 100 μm, mean±SD, biological replicates n=5, *$p<0.05$, **$p<0.01$ vs. control.

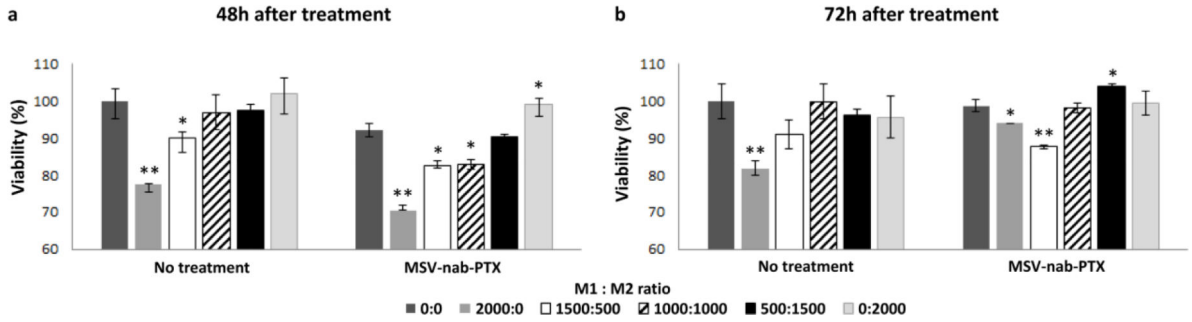

Fig 2.

Viability of breast cancer cells growing in tumor spheres representing hypo-vascularized BCLM in 3D co-culture with *M*1 and *M*2 polarized macrophages. *M*1 macrophages were CRISPR-RICTOR-liposome treated and differentiated in the presence of IFN-gamma/LPS, while *M*2 macrophages were polarized *in vitro* in the presence of IL-4/M-CSF. The viability is shown as a function of varying ratios of *M*1:*M*2 macrophages under conditions of no treatment or exposure to MSV-nab-PTX for (A) 48h and (B) 72h. The varying ratios mimic the varying strength of a hypothetical polarization regimen that shifts this ratio. Mean±SD, biological replicates n=5, *p<0.05, **p<0.01 vs control.

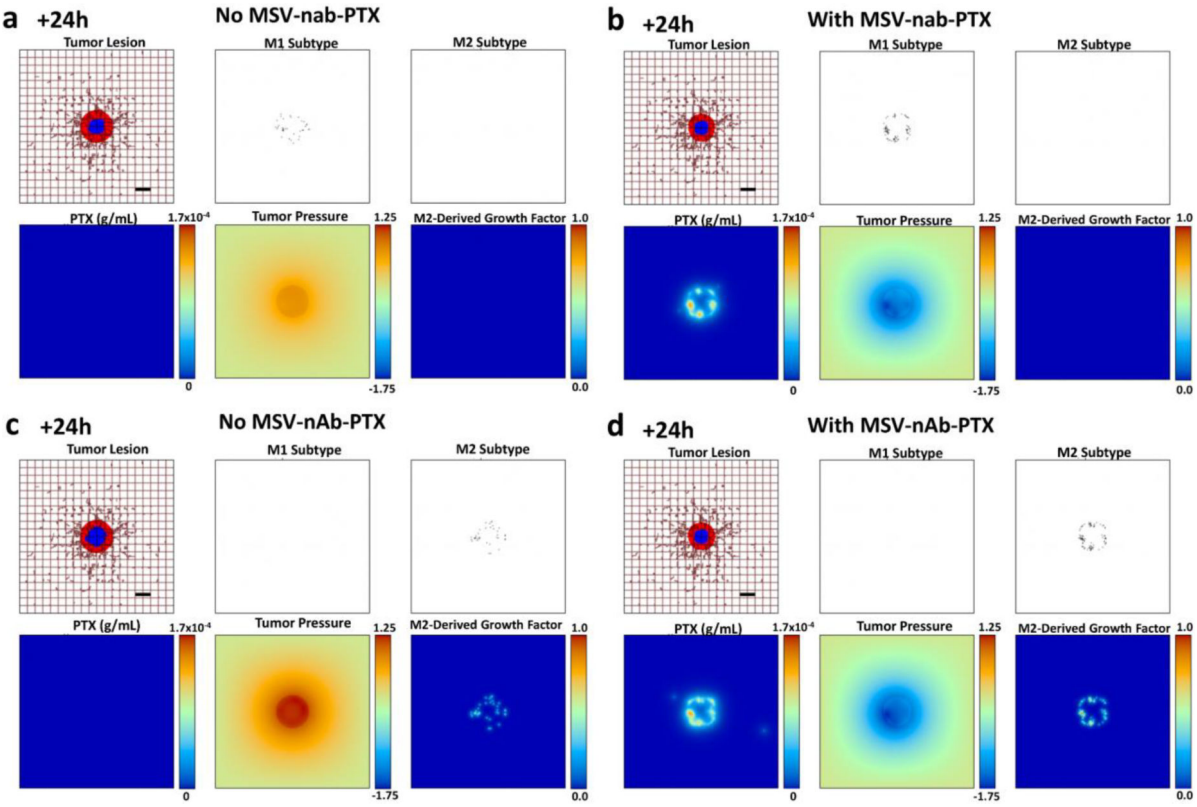

Fig 3.

Simulation of polarized macrophage activity on a growing BCLM lesion at 24h post initiation. (a) *M*1-only, without MSV-nab-PTX treatment; (b) *M*1-only, with MSV-nab-PTX shown. (c) *M*2-only, without MSV-nab-PTX treatment; (d) *M*2-only, with MSV-nab-PTX. As the lesion shrinks during treatment (with viable tumor tissue (red) enclosing a hypoxic region (blue) without necrosis), the oncotic pressure (non-dimensional units) due to cell proliferation correspondingly decreases. The dense liver capillary network is modeled by the rectangular grid (brown), with irregular sprouts generated through angiogenesis during the lesion progression. The *M*2-derived growth factor (non-dimensional units) is only present for the *M*2 case. Bar= 200 μm.

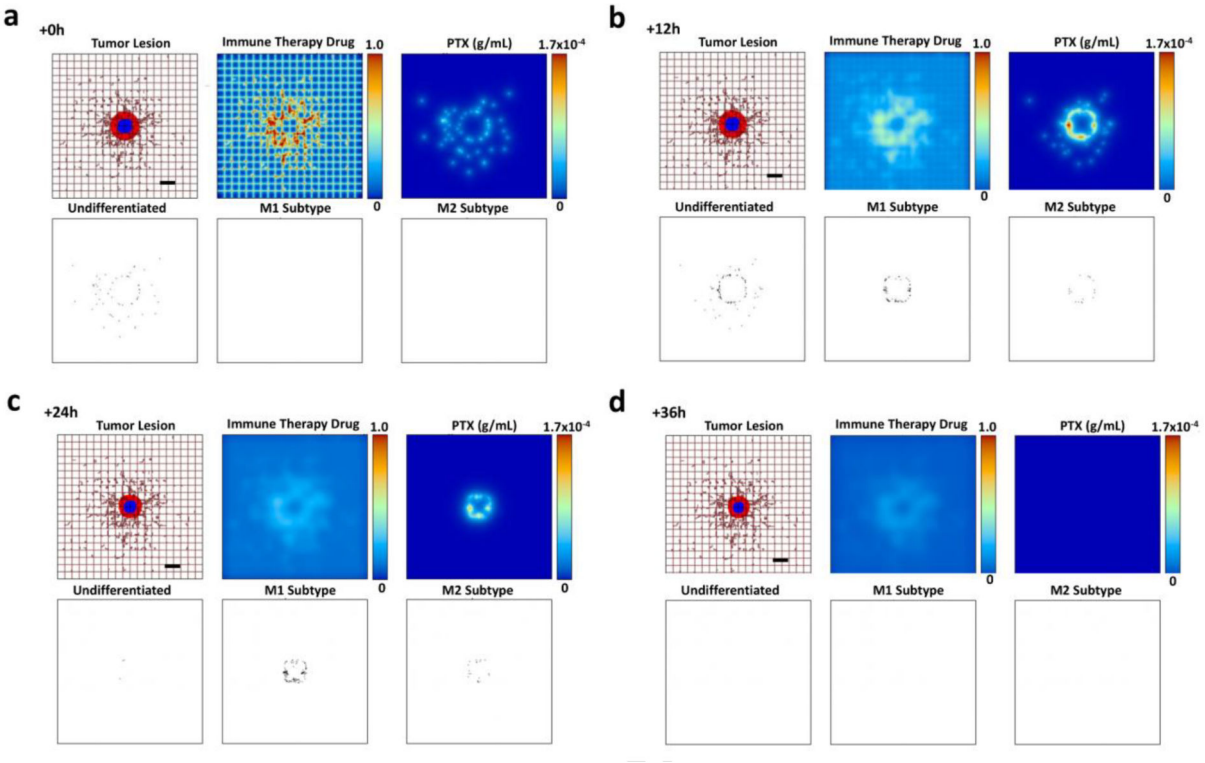

Fig 4.

Simulated progression over 36h (a through d) of a representative tumor lesion after exposure to a medium strength (λ^{N}_{effect} = 280) of a hypothetical "agent affecting macrophage polarization" (AAMP), simulating an immune therapeutic (as a fraction of the maximum in the vasculature) shifting the *M*1:*M*2 ratio to 3.0:1, in conjunction with a bolus injection of MSV-nab-PTX drug-loaded nanoparticles. Colors as in Fig 3. Bar= 200 μm.

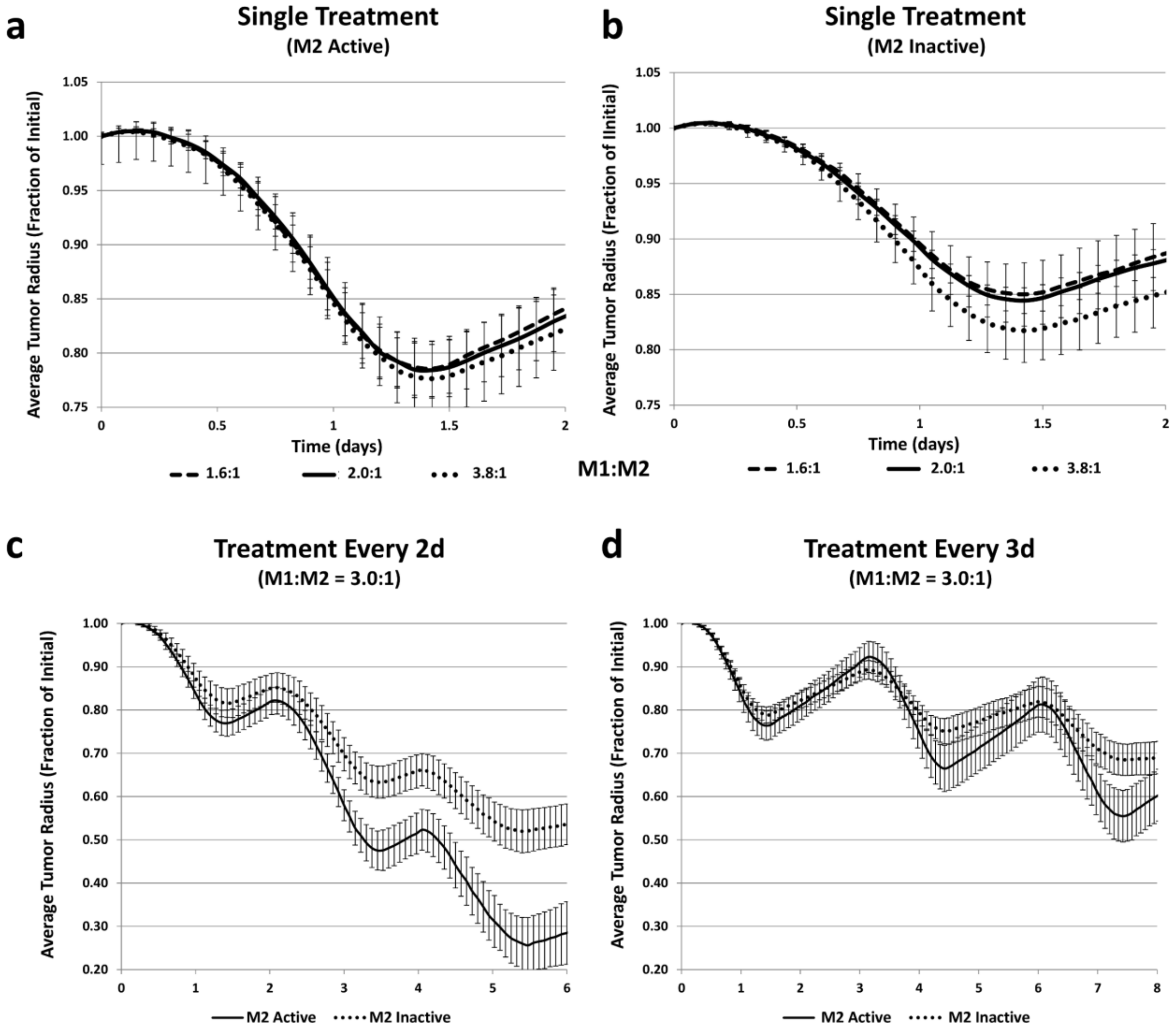

Fig 5.

Simulated average tumor radius (n=5, mean±SD) over time when treated with MSV-nab-PTX loaded macrophages. (a) Single treatment with both *M*1 and *M*2 subtypes active for three different *M*1:*M*2 ratios; (b) Single treatment with only *M*1 active for three different *M*1:*M*2 ratios; (c) Treated every 2d with *M*1:*M*2 of 3.0:1; (d) Treated every 3d with *M*1:*M*2 of 3.0:1.

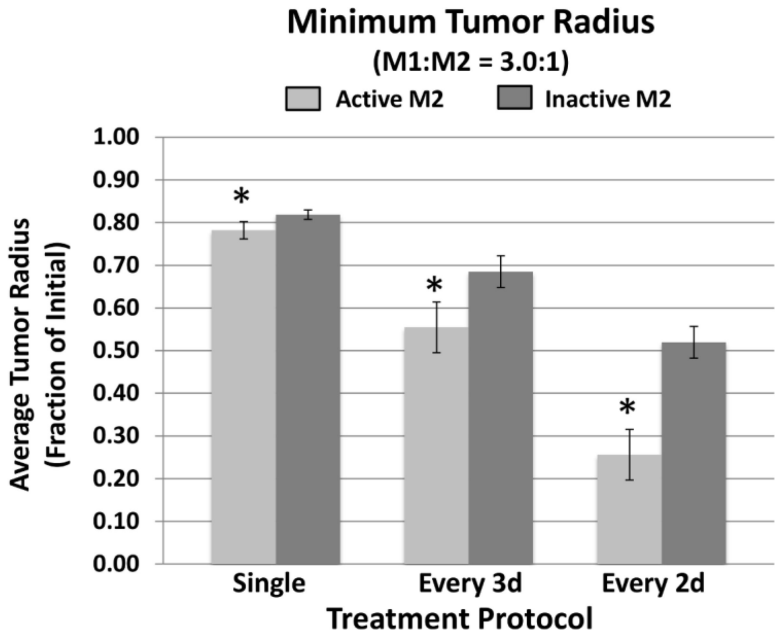

Fig 6.

Simulated minimum tumor radius achieved by the MSV-nab-PTX bolus injection for three treatment protocols in the case of an *M*1:*M*2 ratio of 3.0:1. Simulation results (n=5, mean ±SD) are shown for single dose, administration every 3d, and administration every 2d. (*$p < 0.05$).